Geophysical Research Letters

RESEARCH LETTER
10.1029/2020GL087237

Key Points:
- Lipid biomarker record from Mississippi River floodplain lake sediments spans last 1,800 years
- Lipids and plant wax hydrogen isotopes reconstruct temperature and warm-season moisture
- Medieval (CE 1000–1600) droughts and floods correspond to elevated temperatures and warm-season moisture

Supporting Information:
- Supporting Information S1
- Data Set S1

Correspondence to:
S. E. Muñoz,
s.munoz@northeastern.edu

Citation:
Muñoz, S. E., Porter, T. J., Bakkelund, A., Nusbaumer, J., Dee, S. G., Hamilton, B., et al. (2020). Lipid biomarker record documents hydroclimatic variability of the Mississippi River basin during the Common Era. *Geophysical Research Letters*, *47*, e2020GL087237. https://doi.org/10.1029/2020GL087237

Received 24 JAN 2020
Accepted 26 MAY 2020
Accepted article online 30 MAY 2020

Lipid Biomarker Record Documents Hydroclimatic Variability of the Mississippi River Basin During the Common Era

Samuel E. Muñoz[1,2], Trevor J. Porter[3], Aleesha Bakkelund[3], Jesse Nusbaumer[4], Sylvia G. Dee[5], Brynnydd Hamilton[1], Liviu Giosan[6], and Jessica E. Tierney[7]

[1]Department of Marine and Environmental Sciences, Marine Science Center, Northeastern University, Nahant, MA, USA, [2]Department of Civil and Environmental Engineering, Northeastern University, Boston, MA, USA, [3]Department of Geography, University of Toronto, Mississauga, Ontario, Canada, [4]Climate and Global Dynamics Laboratory, NCAR, Boulder, CO, USA, [5]Department of Earth, Environmental, and Planetary Sciences, William Marsh Rice University, Houston, TX, USA, [6]Department of Geology and Geophysics, Woods Hole Oceanographic Institution, Woods Hole, MA, USA, [7]Department of Geosciences, University of Arizona, Tucson, AZ, USA

Abstract Floods and droughts in the Mississippi River basin are perennial hazards that cause severe economic disruption. Here we develop and analyze a new lipid biomarker record from Horseshoe Lake (Illinois, USA) to evaluate the climatic conditions associated with hydroclimatic extremes that occurred in this region over the last 1,800 years. We present geochemical proxy evidence of temperature and moisture variability using branched glycerol dialkyl glycerol tetraethers (brGDGTs) and plant leaf wax hydrogen isotopic composition (δ^2H_{wax}) and use isotope-enabled coupled model simulations to diagnose the controls on these proxies. Our data show pronounced warming during the Medieval era (CE 1000–1,600) that corresponds to midcontinental megadroughts. Severe floods on the upper Mississippi River basin also occurred during the Medieval era and correspond to periods of enhanced warm-season moisture. Our findings imply that projected increases in temperature and warm-season precipitation could enhance both drought and flood hazards in this economically vital region.

Plain Language Summary The Mississippi River basin is an economically vital region for industry and agriculture, but it is prone to disruptive flooding and drought. Here we use organic molecules preserved in a lake sediment core to reconstruct the temperature and seasonal moisture patterns of the last 1,800 years. Our reconstruction shows that the Medieval period (ca. CE 1000–1,600) was relatively warm and that warmer temperatures in this region are associated with increased frequencies of severe droughts and floods. These findings generally support climate model projections of increasing drought and flood hazard in the Mississippi River basin as a result of anthropogenic climate change.

1. Introduction

The Mississippi River basin is an economic cornerstone of the United States, providing freshwater, hydroelectric power, transportation, and farmland to the North American continental interior. Hydroclimatic extremes—both floods and droughts—within the Mississippi River basin are responsible for some of the costliest and most consequential natural disasters of the last century (Barry, 2007; Camillo, 2012; Cook, 2019; Cook et al., 2007). These events damage infrastructure, destroy crops, disrupt shipping, and displace communities, so understanding their sensitivity to climate variability and change is critical for hazard forecasting, mitigation, and infrastructure planning (Cook et al., 2015; Munoz & Dee, 2017; Shadie et al., 2018).

Extreme events occur infrequently, and proxy-based reconstructions of past floods and droughts in the Mississippi River basin have proven effective in establishing the range of natural hydroclimatic variability during the Common Era. These reconstructions document pronounced shifts in the frequency of midcontinental floods and droughts, particularly during the Medieval era (ca. CE 1000–1600), which included elevated frequencies of both high-magnitude floods (Harden et al., 2015; McQueen et al., 1993; Munoz et al., 2015; Wang & Leigh, 2012) and severe and persistent droughts (Cook et al., 2004; Mason et al., 2004; Miao et al., 2007; Woodhouse & Overpeck, 1998). Analyses of coupled model simulations and data

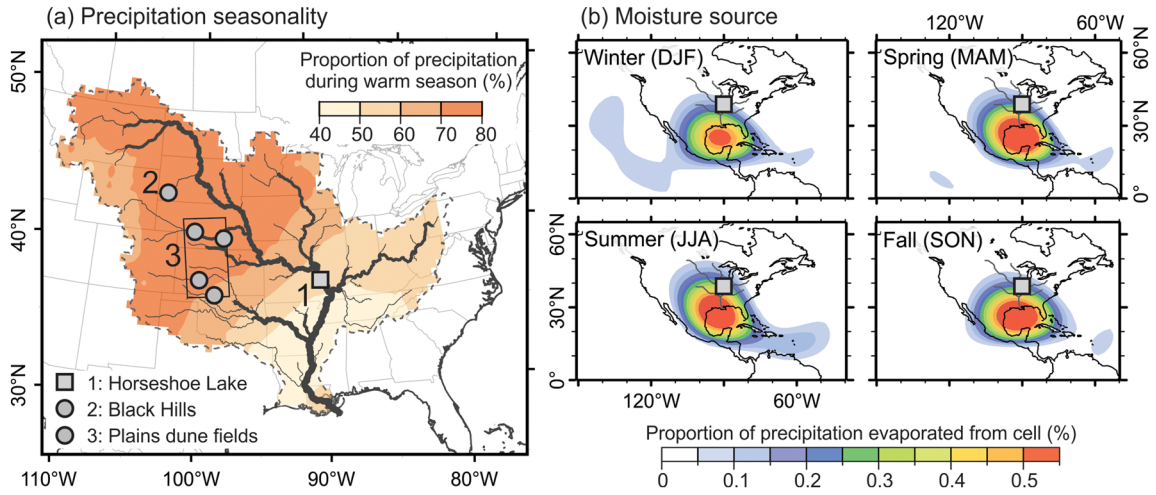

Figure 1. Hydroclimatology (CE 1980–2015) of the Mississippi River basin: (a) precipitation seasonality, expressed as a proportion of total annual precipitation falling during March–August (Global Precipitation Climatology Center data; Schneider et al., 2011), showing sites mentioned in text (1) Horseshoe Lake (this study) and upper Mississippi River paleoflood sites (Munoz et al., 2015), (2) Black Hills paleoflood sites (Harden et al., 2015), and (3) dune activation sites (Hanson et al., 2010); (b) moisture source of seasonal precipitation at Horseshoe Lake simulated using GISS ModelE2.1.

assimilation products emphasize the role of ocean-atmosphere coupling, radiative forcing, and land-surface feedbacks in the formation of midcontinental droughts (Coats et al., 2016; Cook et al., 2007; Cook et al., 2009, 2014; Feng et al., 2008; Steiger et al., 2019) and pluvials (Cook, Cook, et al., 2011; Cook, Seager, & Miller, 2011; Munoz & Dee, 2017; Seager et al., 2005), though uncertainty remains over the climatic conditions that enhance or suppress the occurrence of hydroclimatic extremes in this region (Ault et al., 2018; Coats et al., 2016). A critical need, then, is an independent reconstruction of regional temperature and moisture that can be used to evaluate the hydroclimatology of the Mississippi River basin in relation to extreme events.

Here we address this need with a new 1,800 year lipid biomarker lake sediment record situated near the center of the Mississippi basin (Horseshoe Lake, Illinois, USA) that we use to reconstruct regional hydroclimatic variability over the late Holocene (Figure 1). In our study region, intra-annual variability in the isotopic value of precipitation reflects both air temperature and moisture source (Sjostrom & Welker, 2009; Tian et al., 2018). To disentangle the relationships between temperature, precipitation, and water isotopes, we combine the hydrogen isotope composition of the long-chain waxy molecules from plant leaves (δ^2H_{wax}) with an independent temperature reconstruction derived from branched glycerol dialkyl glycerol tetraethers (brGDGTs). We then couple this multibiomarker record with output from isotope-enabled global climate models to diagnose the controls on these proxies. Finally, we compare our paleoclimate reconstruction to a regional network of paleohydrologic records to evaluate the roles of temperature and moisture on flood and drought hazards.

2. Materials and Methods

2.1. Sediment Cores and Chronology

Our multibiomarker record is derived from sediment cores collected from the infilling thalweg of Horseshoe Lake (90.081279°W, 38.704767°N, water depth 1.09 m) in 2012 using a Livingston-Wright piston corer. A 440-cm-long composite of these cores (HORM12) has been used to develop paleoecological (Brugam & Munoz, 2018; Munoz et al., 2014), paleodemographic (White et al., 2018, 2019), and paleoflood (Munoz et al., 2015, 2019) records. Here, we use a modified version of the HORM12 age-depth model described by Munoz et al. (2014) that is based on a spline implemented in Clam v.2.2 (Blaauw, 2010) constrained by nine accelerator mass spectrometry ^{14}C dates on terrestrial plant macrofossils and the core top. We modified this original chronology using ^{210}Pb, ^{214}Pb, and ^{137}Cs activities collected in a Canberra Broad Energy Germanium Detector on 12 dried and powdered sediment samples (Figure S1 in the supporting information). We then used the constant rate of supply model (CRS; Appleby, 2002) with a reference level based

on the ^{137}Cs peak to estimate ages and confidence intervals of the eight samples with excess ^{210}Pb and integrated these ages into the age model (Figure S2).

2.2. Lipid Extraction

For δ^2H_{wax} and brGDGT analysis we selected 34 samples that span the length of the core, where samples integrate 1–2 cm of core depth. Since its formation, Horseshoe Lake has received extralocal sediment from the Mississippi River during at least eight large flood events identified by Munoz et al. (2015, 2019). We limited our sampling for lipid biomarkers to material sourced from the local catchment.

Soil-bound lipids were extracted from lyophilized sediments by microwave-assisted heating or accelerated solvent extraction. The total lipid extract was condensed under high-purity N_2 gas and separated by column chromatography into neutral (brGDGT) and acid fractions using an aminopropylsilyl-gel column and 2:1 (v/v) dichloromethane:isopropanol and 4% acetic acid in dichloromethane or 4% formic acid in diethyl ether as eluents. Both fractions were condensed under dry N_2 gas. The brGDGT fraction was redissolved in 99:1 (v/v) hexanes:isopropanol and filtered through a 0.45 μm PTFE filter prior to analysis. The n-acid fraction was methylated to produce Fatty Acid Methyl Esters (FAMEs) using a methanol of known isotopic composition in hydrochloric acid (19:1 v/v) heated to 70°C for 12 hr. FAMEs were recovered by liquid-liquid extraction (dissolution in hexanes) and passed through a 5% deactivated Si-gel column, eluting any nonpolar compounds with hexanes and the FAME fraction with dichloromethane. FAMEs were quantified by Gas Chromatography (Thermo Trace 1310) with a Flame Ionization Detector (GC-FID), Programmable Temperature Vaporizing (PTV) injector and a Rxi-5-ms column (30 m × 0.25 mm, 1-μm film). Peak areas were used to calculate the modal chain length (C_{max}), Average Chain Length ($ACL = \sum(C_n \times {}_n)/\sum C_n$, where C_n is the abundance of even chain lengths from $C_{20\text{-}32}$ and n is chain number), and the Carbon Preference Index ($CPI = [\sum C_{20,22,24,26,28,30} + \sum C_{22,24,26,28,30,32}]/[2 \times \sum C_{21,23,25,27,29,31}]$).

2.3. Hydrogen Isotopic Analyses

To reconstruct moisture trends, we analyzed the δ^2H_{wax} of n-C_{24}, n-C_{26}, and n-C_{28} acids. Trends in δ^2H_{wax} of all chain lengths are similar (supporting information (SI) data set), so we focus our analyses on n-C_{28} acids as these are the most abundant n-acid in our core and can be attributed to terrestrial plants (Sachse et al., 2012). The δ^2H_{wax} values were measured by GC-IRMS (Thermo Delta V Plus) relative to a reference H_2 gas, and calibrated to the VSMOW-SLAP scale using the A6 alkane standard (A. Schimmelmann at Indiana University). Samples were analyzed in at least duplicate and averaged to yield an overall precision of 2‰. Calibrated δ^2H_{wax} values were then corrected by mass balance to account for the three H atoms added to the FAME molecule during the methylation step. The methanol δ^2H was determined by methylating a phthalic acid of known isotopic composition (Schimmelmann, Indiana University) following the method of Lee et al. (2017).

2.4. GDGT Analyses

To reconstruct temperature trends, brGDGTs were analyzed by HPLC-MS (Agilent 6120) in single ion monitoring mode and quantified by comparison to an internal C46 brGDGT standard. Chromatographic separation was achieved with two BEH HILIC silica columns (2.1 × 150 mm, 1.7 μm; Waters) as recommended by Hopmans et al. (2016). The brGDGT relative abundances were used to calculate the temperature-sensitive $MBT'5_{Me}$ index (De Jonge et al., 2014): $MBT'5_{Me} = [Ia + Ib + Ic]/[Ia + Ib + Ic + IIa + IIb + IIc + IIIa]$, where Types I, II, and III brGDGTs have tetra-, penta-, and hexa-methylated groups, respectively, and Types a, b, and c have 0, one and two rings, respectively. $MBT'5_{Me}$ estimates are precise to ±0.007 (1σ) based on long-term analysis of a laboratory external standard. Mean annual air temperatures were calculated from the downcore $MBT'5_{Me}$ record using the Russell et al. (2018) calibration, which has a RMSE of 2.4°C.

2.5. Isotope-Enabled Climate Models

Given the sensitivity of the hydrogen isotopic composition of precipitation (δ^2H_p) to moisture source and temperature in our study region, we used global climate models to (1) examine the seasonal variability in the source of moisture delivered to Horseshoe Lake and (2) diagnose controls on δ^2H_{wax} and brGDGT records in relation to seasonal and annual trends in surface temperature and the hydrogen isotopic composition of precipitation (δ^2H_p).

To evaluate the seasonal variability of moisture source, we used the NASA GISS ModelE2.1 climate model equipped with numerical water tracers (Nusbaumer et al., 2019). This model allows for the tracking of moisture in a simulated atmosphere from its evaporation source to the point of precipitation over a particular site. These simulations match observations of climatological precipitation amount and column water vapor over the study region (Schmidt et al., 2014). The simulation was run for the period CE 1980–2015 using observed sea surface temperatures and sea ice, while the horizontal winds were nudged to the Modern-Era Retrospective analysis for Research and Applications, Version 2 (MERRA2) reanalysis, in order to match the observed atmospheric circulation as closely as possible.

To evaluate the δ^2H_{wax} and brGDGT records, we compared their trends to output from the water isotope-enabled NCAR Community Earth System Model Version 1 (iCESM1) (Brady et al., 2019) Last Millennium Ensemble (Stevenson et al., 2019). From iCESM1, we extracted monthly surface temperature, precipitation, and δ^2H_p values for the period CE 850–2005 from the grid cell closest to Horseshoe Lake for all three "full forcing" model runs available, as well as the orbital-only and greenhouse gas-only (GHG-only) model runs, and computed annual, warm- (March–August) and cold-season (September–April) means. This definition of warm-season encompasses hydrologic maxima and the growing season in our study region. To facilitate data-model comparison, we smoothed annual and seasonal values using a 51-year moving mean to reflect mixing and time averaging of the sedimentary archive; we resampled ($n = 100$) this smoothed series within the 2σ chronological uncertainty for each proxy sample to estimate uncertainty in the data-model comparison.

3. Results and Discussion

3.1. Modern Controls on Moisture and δ^2H_p

Under modern circulation patterns (CE 1980–2015), ~60% of precipitation at Horseshoe Lake falls in the warm season (March–August), with a warm-season bias in precipitation increasing with distance from the Gulf of Mexico (Figure 1a). This warm-season precipitation is enriched in ^2H (March–August $\delta^2H = -19‰$) compared to the cold-season (September–February $\delta^2H = -47‰$) (Bowen, 2019). Moisture sourced from the Gulf of Mexico is enriched in ^2H compared to moisture from the Atlantic and Pacific oceans (Sjostrom & Welker, 2009), so separating the influences of seasonality and source on water isotopes in this region has been challenging (Bird et al., 2017; Tian et al., 2018). Our moisture source analyses implemented in GISS ModelE2.1 demonstrate that, under modern conditions, the Gulf of Mexico is the dominant source of precipitation to Horseshoe Lake across all seasons (Figure 1b). In winter (December–February, DJF), there is a small proportion of precipitation sourced from the Pacific Ocean, while in spring (March–May, MAM) and summer (June–August, JJA) some precipitation originates from the tropical Atlantic and the continent itself. The stability of the moisture source origin implies that changes in δ^2H_p in our study area will primarily reflect seasonal processes that affect evaporation and moisture advection from the Gulf of Mexico rather than changes in moisture source.

3.2. Controls on Plant Waxes

The δ^2H_{wax} is influenced by δ^2H_p (i.e., precipitation derived source water) and the community of plants contributing waxes to the fossil record which can influence the average net fractionation of H isotopes between waxes and source water ($\varepsilon_{wax\text{-}water}$) (Sachse et al., 2012). The latter can be a major uncertainty in δ^2H_{wax}-based hydroclimate reconstructions; however, local pollen data confirm there were no major paleoflora turnovers, with arboreal taxa accounting for ~50–90% of the pollen sum (Munoz et al., 2014), indicative of a paleoflora predominantly composed of trees and shrubs (Williams & Jackson, 2003). A simple analysis of core top (approximately modern) δ^2H_{wax} (−126‰) and plausible source water δ^2H assumptions bracketing mean annual to March–August (warm-season) precipitation ($\delta^2H_p = -33‰$ to −19‰; Bowen, 2019) suggests a probable $\varepsilon_{wax\text{-}water}$ range of −107‰ to −93‰, which is consistent with εC_{29} alkane-water values observed in shrubs (−99‰ ± 32‰) and trees (−121‰ ± 22‰) globally (Sachse et al., 2012). The Horseshoe Lake record is dominated by even chain length n-acids (CPI $\bar{x} = 5.1 \pm 1.5$), indicating a terrestrial plant source (Eglinton & Hamilton, 1967). We observe a mean ACL of 27.4 ± 0.2, no downcore trend in ACL ($R^2 = 0.01$, $\nu = 33$, $t = -0.53$, $p = 0.60$), and a constant C_{28} modal chain-length for all samples (SI dataset). Complacency in these wax traits supports the notion of a stable assemblage of plants contributing to the

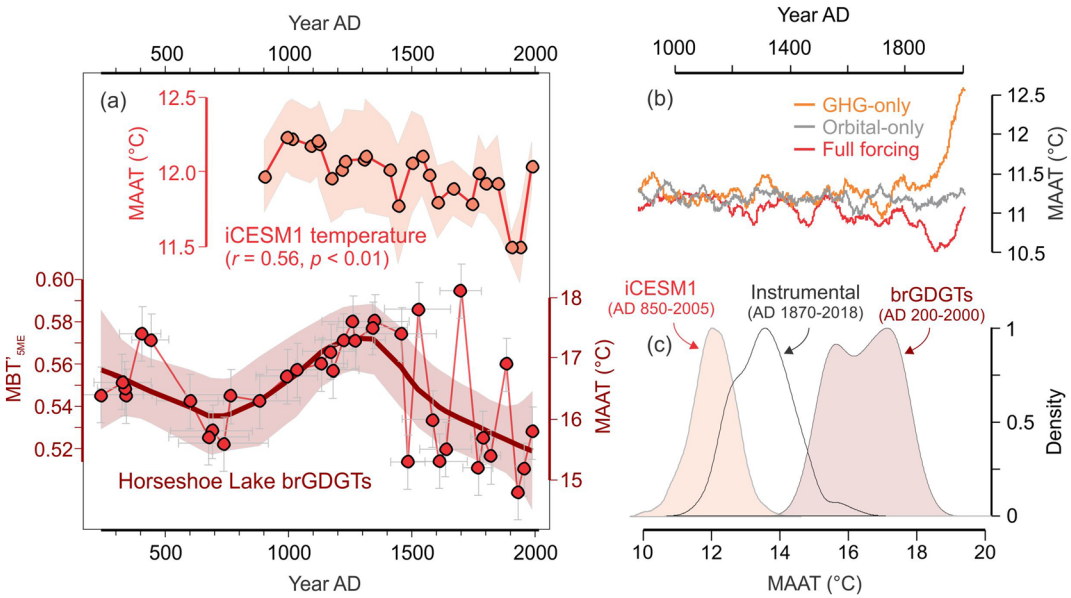

Figure 2. Reconstructed and simulated climate at Horseshoe Lake: (a) brGDGT MBT'$_{5ME}$ index (bottom; data points indicate the 2σ analytical precision and age-model confidence interval, thick line shows Loess curve with 2σ regression uncertainty, and secondary axis shows mean annual air temperature (MAAT) estimated from MBT'$_{5ME}$ with a RMSE of 2.4°C) and simulated MAAT sampled on reconstructed years from the iCESM1 "full forcing" model run (top; shading shows 1σ resampling confidence interval); (b) iCESM1 simulated mean annual temperature (51-year moving mean) under three forcing scenarios; (c) density plots of simulated (iCESM1), reconstructed (brGDGTs), and instrumental mean annual temperature (National Weather Service, NWS, 2020).

sedimentary wax record. As such, we assume that $\varepsilon_{wax\text{-}water}$ did not vary significantly through time and interpret δ^2H_{wax} primarily as a proxy for δ^2H_p.

3.3. Temperature Reconstruction

Mean annual temperatures reconstructed from the MBT'5$_{Me}$ index range from 14.8–18.1°C, including a temperature maximum between CE 1000–1600 ($\bar{x}$ = 17.1°C) bracketed by minima around CE 500–1000 ($\bar{x}$ = 16.2°C) and 1600–1900 ($\bar{x}$ = 15.8°C) (Figure 2a). The reconstruction tracks iCESM1 simulated mean annual temperatures (r = 0.53, t = 3.25, ν_{eff} = 19.32, p < 0.01), showing warmer temperatures between CE 1000–1600 that generally cool toward present. We also found significant correlations between reconstructed temperatures and warm- and cool-season temperature averages simulated in iCESM1 (Table S1). Reconstructed temperatures exhibit increased variability after CE 1400 that is not simulated in iCESM1, possibly reflecting altered source contributions of brGDGTs associated with extralocal sediment input during floods. Both reconstructed and simulated temperatures show late twentieth century warming that does not exceed temperatures of the Medieval period, and the simulation experiments show that this modern warming is driven by greenhouse gas forcing (Figure 2b). Absolute temperatures differ among simulated ($\bar{x}$ = 12.0°C; s = 0.65°C), reconstructed ($\bar{x}$ = 16.5°C; s = 0.88°C), and instrumental temperatures for the period CE 1870–2018 ($\bar{x}$ = 13.5°C; s = 0.82°C; National Weather Service, NWS, 2020) (Figure 2c). Instrumental temperatures fall within the 1σ prediction interval (±2.4°C) of reconstructed temperatures for the 20th century ($\bar{x}$ = 15.3°C), implying that part of the offset between reconstructed and instrumental temperatures is due to the short temporal span of the instrumental data and calibration error of the MBT'5$_{Me}$ record. The disparity between instrumental temperature magnitudes and that simulated in iCESM1 has been noted elsewhere (Ault et al., 2013; Dee et al., 2017; Parsons et al., 2017). The consistency in trends between observed and simulated temperatures over the late Holocene—and the clear emergence of a regionally warm Medieval period—is notable and implies that the brGDGTs provide a robust reconstruction of regional trends in mean annual temperature.

3.4. Moisture Reconstruction

The δ^2H_{wax} values span a range of 41‰ over the period of record and show a minimum between CE 500–1000 ($\bar{x}$ = −158.0‰), followed by moderate enrichment between CE 1000–1600 ($\bar{x}$ = −151.0‰) and

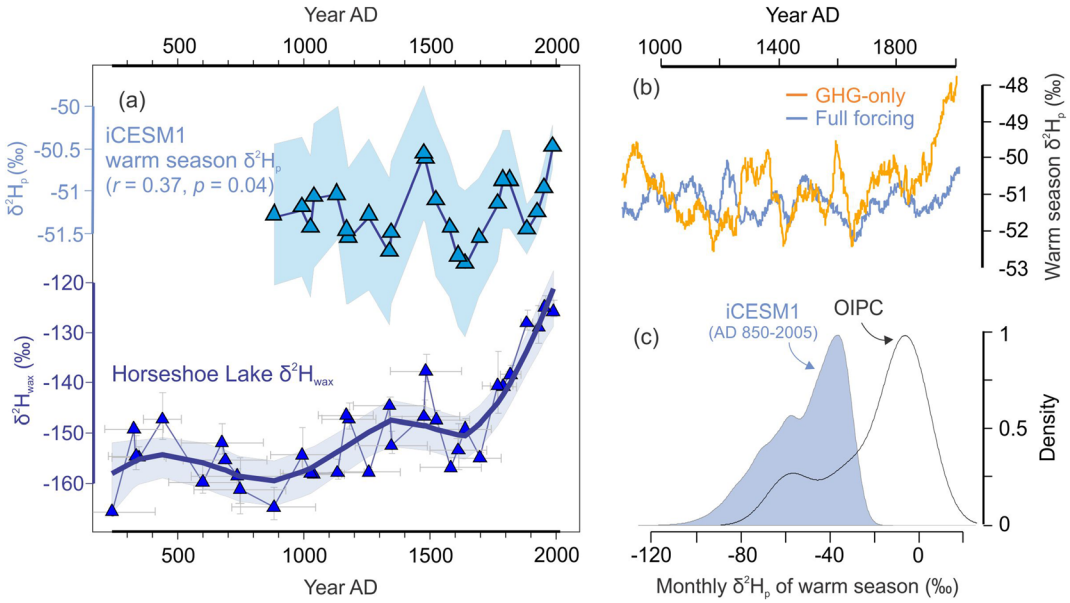

Figure 3. Horseshoe Lake δ^2H_{wax} and simulated warm-season (March–August) δ^2H_p: (a) δ^2H_{wax} values (bottom; data points show 2σ confidence intervals; thick line shows Loess curve with 2σ confidence intervals of the local regression) and simulated (iCESM1) warm-season δ^2H_p (top) sampled on reconstructed years where shading shows 2σ confidence intervals of re-sampling; (b) iCESM1 simulated warm-season δ^2H_p (51-year moving mean) under two forcing scenarios; (c) density plots of simulated (iCESM1) and observed (OIPC; Bowen, 2019) monthly δ^2H_p during the warm season.

pronounced enrichment that begins around CE 1700 and increases further after CE 1885 ± 23 years ($\bar{x}$ = −126.9‰) to its highest values of the Common Era (Figure 3a). We compared these δ^2H_{wax} trends to δ^2H_p simulated in iCESM1 and found the strongest correlation with warm-season (March–August) δ^2H_p ($r = 0.37$, $t = 1.89$, $\nu_{eff} = 13.41$, $p = 0.04$), while correlation to cold-season (September–February) δ^2H_p is negative ($r = -0.36$, $t = -1.82$, $\nu_{eff} = 12.28$, $p = 0.05$) (Table S1). Simulations of warm-season δ^2H_p in the "full-forcing" runs of iCESM1 show only a moderate isotopic enrichment over the last century, but the experimental runs imply that greenhouse forcing drives its recent enrichment (Figure 3b). We note that simulated warm-season δ^2H_p in iCESM1 ($\bar{x}$ = −51.2‰, s = 17.1‰) underestimates empirically constrained estimates of warm-season δ^2H_p for this site ($\bar{x}$ = −19‰, s = 22‰; Bowen, 2019) (Figure 3c). The data-model comparisons for hydrogen isotope composition imply that δ^2H_{wax} at Horseshoe Lake is sensitive to warm-season δ^2H_p, a variable that is strongly influenced by air temperatures in both our study region (Tian et al., 2018) and the midlatitudes in general (Rozanski et al., 1993).

To assess the role of air temperature in driving δ^2H_{wax} variations at Horseshoe Lake, we compare the leaf wax record to our independent temperature reconstruction from brGDGTs (Figure 4). We found that if these data are smoothed to accentuate centennial-scale trends, reconstructed temperatures track δ^2H_{wax} until the seventeenth century ($r = 0.56$, $t = 3.20$, $\nu_{eff} = 2.99$, $p < 0.02$), when temperatures and δ^2H_{wax} values decouple and shift to low and high extremes, respectively. The centennial-scale coupling between reconstructed temperatures and δ^2H_{wax} throughout most of the record is consistent with observations linking higher temperatures to the enrichment of ^2H in precipitation (Tian et al., 2018) under a constant set of boundary conditions. The decoupling of temperature and δ^2H_{wax} is driven by the four uppermost samples that are enriched by ~25‰ relative to prior centuries. This pronounced enrichment may be caused by a relative increase in warm-season precipitation that has been observed in this region over the twentieth century and attributed to greenhouse forcing (Dai et al., 2016; Easterling et al., 2017; Peterson et al., 2013). This implies that modern spatial patterns of precipitation seasonality and source region reflect a recent enhancement of warm-season moisture transport from the Gulf of Mexico into the continental interior. Ultimately, the relationships reported here between temperature, moisture, and δ^2H_{wax} indicate that our leaf wax record reflects both temperature and the relative amount of warm-season precipitation throughout the entire period of record.

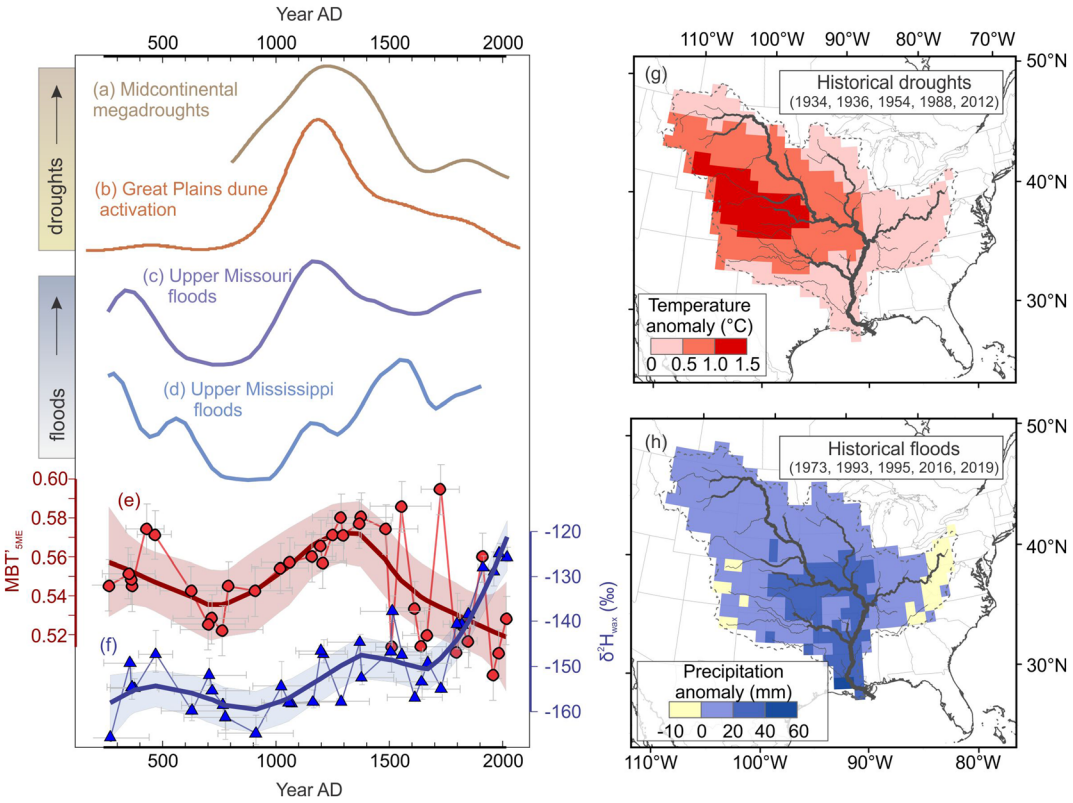

Figure 4. Regional synthesis of paleohydrologic records from the Mississippi River basin. Normalized probability density functions of (a) midcontinental (32–46°N, 105–90°W) megadrought events (≥10 consecutive years PDSI ≤ −0.5; Cook et al., 2010); (b) Great Plains dune activation (Forman et al., 2008; Hanson et al., 2009, 2010); (c) slackwater paleoflood deposits from the Black Hills, upper Missouri River basin (Harden et al., 2015); (d) upper Mississippi River floodplain paleoflood deposits (Munoz et al., 2015); (e) brGDGT-temperature records; and (f) δ^2H_{wax} from Horseshoe Lake, Illinois (this study). Anomalies of (g) mean annual temperature (Compo et al., 2011) associated with five severe historical midcontinental droughts and (h) warm-season (March–August) precipitation (Schneider et al., 2011) associated with five severe historical floods at the Mississippi River gage at St. Louis, Missouri (07010000).

3.5. Implications for Hydroclimatic Extremes

Our reconstruction of temperature and warm-season moisture from Horseshoe Lake provides insight into the role of hydroclimatic variability in regulating the occurrence of drought and floods in the Mississippi River basin (Figure 4). Temperature and soil moisture at Horseshoe Lake are highly autocorrelated across the Mississippi River basin (Figure S3). The brGDGT-based temperature reconstruction provides independent support for the relationship between positive surface temperature anomalies and the severe and frequent Medieval-era droughts in the midcontinent (32–46°N, 105–90°W) inferred from tree ring (Figure 4a) and dune activation (Figure 4b) records. These reconstructions show the highest rates of drought occurrence between circa CE 1000–1600, corresponding closely with the temperature maximum in our brGDGT record (Figure 4e). As midcontinental temperatures cooled following their Medieval era maximum, the frequency of severe midcontinental drought declined. This relationship between high temperatures and drought is consistent with the most severe historical droughts (Figure 4g) and is the basis for projections of more severe and frequent midcontinental droughts under continued greenhouse gas forcing (Ault et al., 2016; Cook et al., 2015).

In contrast to drought and its association with surface temperature, flood occurrence during the Common Era track the δ^2H_{wax}-based reconstruction of relative warm-season moisture and temperature (Figure 4). Paleoflood records of high-magnitude events from the upper Missouri River basin (Figure 4c) and the upper Mississippi River (Figure 4d) exhibit coherent trends, and show an interval of low flood frequency between circa CE 500 and 1000 that corresponds to the most depleted δ^2H_{wax} values of our record (Figure 4f), while enrichment of δ^2H_{wax} before CE 500 and after CE 1000 is associated with increased flood frequency. Flooding did not decline as temperatures cooled following the Medieval era, implying that warm-season

moisture exerts a primary control on flood occurrence on the upper Mississippi River basin (Dirmeyer & Kinter, 2009; Knox, 1988; Kunkel et al., 1994; Wise et al., 2018)—consistent with precipitation anomalies observed during historical floods (Figure 4h). The close coupling we find between our reconstruction of relative warm-season precipitation and flood occurrence on the upper Mississippi and Missouri Rivers during the Common Era supports model-based projections of increased flood hazard in these basins under continued greenhouse gas forcing (Milly et al., 2002; Qiao et al., 2014; Wise et al., 2018), though changes in land-cover and river management also play a fundamental role in modulating flood hazard (Munoz et al., 2018; Pinter et al., 2008; Tao et al., 2014).

4. Conclusions

Our new lipid biomarker record reconstructs temperature and moisture variability in the Mississippi River basin over the last 1,800 years. These data document pronounced Medieval era warming (ca. CE 1000–1600) that corresponds to a period of enhanced midcontinental drought frequency and severity, implying that regionally warm temperatures played a fundamental role in the formation of severe Medieval era droughts (Coats et al., 2016; Steiger et al., 2019)—and providing support for projections of increasing drought hazard in this region under continued greenhouse forcing (Ault et al., 2016; Cook et al., 2015). We show that severe floods on the upper Mississippi basin also occurred during the Medieval period, corroborating projections of enhanced flood and drought hazards in this region over the next century.

Data Availability Statement

Data in this study are available in the SI data set and through the Paleoclimate Branch of NOAA NCEI (at https://www.ncdc.noaa.gov/paleo-search/study/29832).

Acknowledgments

We thank David Carter and Isabella Lopez for laboratory assistance and Ben Bates and three anonymous reviewers for comments on earlier drafts of the manuscript. This project was supported by grants to S. E. M and L. G. (NSF EAR-1804107), T. J. P. (NSERC Discovery Grant), and S. G. D. (NOAA-NA18OAR4310427).

References

Appleby, P. G. (2002). Chronostratigraphic techniques in recent sediments. In W. M. Last, & J. P. Smol (Eds.), *Tracking environmental change using lake sediments* (pp. 171–203). Dordrecht: Springer. https://doi.org/10.1007/0-306-47669-X_9

Ault, T. R., Cole, J. E., Overpeck, J. T., Pederson, G. T., St. George, S., Otto-Bliesner, B., et al. (2013). The continuum of hydroclimate variability in western North America during the last millennium. *Journal of Climate*, *26*(16), 5863–5878. https://doi.org/10.1175/JCLI-D-11-00732.1

Ault, T. R., Mankin, J. S., Cook, B. I., & Smerdon, J. E. (2016). Relative impacts of mitigation, temperature, and precipitation on 21st-century megadrought risk in the American Southwest. *Science Advances*, *2*(10), e1600873.

Ault, T. R., St. George, S., Smerdon, J. E., Coats, S., Mankin, J. S., Carrillo, C. M., et al. (2018). A robust null hypothesis for the potential causes of megadrought in western North America. *Journal of Climate*, *31*(1), 3–24. https://doi.org/10.1175/JCLI-D-17-0154.1

Barry, J. M. (2007). *Rising tide: The great Mississippi flood of 1927 and how it changed America*. New York, NY: Simon and Schuster.

Bird, B. W., Wilson, J. J., Gilhooly, W. P. III, Steinman, B. A., & Stamps, L. (2017). Midcontinental Native American population dynamics and late Holocene hydroclimate extremes. *Scientific Reports*, *7*(1), 41,628. https://doi.org/10.1038/srep41628

Blaauw, M. (2010). Methods and code for 'classical' age-modelling of radiocarbon sequences. *Quaternary Geochronology*, *5*(5), 512–518. https://doi.org/10.1016/j.quageo.2010.01.002

Bowen, G. J. (2019). The online isotopes in precipitation calculator, version OIPC 2.2.

Brady, E., Stevenson, S., Bailey, D., Liu, Z., Noone, D., Nusbaumer, J., et al. (2019). The connected isotopic water cycle in the Community Earth System Model version 1. *Journal of Advances in Modeling Earth Systems*, *11*, 2547–2566. https://doi.org/10.1029/2019MS001663

Brugam, R. B., & Munoz, S. E. (2018). A 1600-year record of human impacts on a floodplain lake in the Mississippi River Valley. *Journal of Paleolimnology*, *60*(3), 445–460. https://doi.org/10.1007/s10933-018-0033-0

Camillo, C. A. (2012). *Divine providence: The 2011 flood in the Mississippi River and tributaries project*. Vicksburg, MS: Mississippi River Commission.

Coats, S., Smerdon, J. E., Karnauskas, K. B., & Seager, R. (2016). The improbable but unexceptional occurrence of megadrought clustering in the American West during the Medieval Climate Anomaly. *Environmental Research Letters*, *11*(7), 074025. https://doi.org/10.1088/1748-9326/11/7/074025

Compo, G. P., Whitaker, J. S., Sardeshmukh, P. D., Matsui, N., Allan, R. J., Yin, X., et al. (2011). The twentieth century reanalysis project. *Quarterly Journal of the Royal Meteorological Society*, *137*(654), 1–28. https://doi.org/10.1002/qj.776

Cook, B. (2019). *Drought: An interdisciplinary perspective*. New York, NY: Columbia University Press. https://doi.org/10.7312/cook17688

Cook, B. I., Ault, T. R., & Smerdon, J. E. (2015). Unprecedented 21st century drought risk in the American Southwest and Central Plains. *Science Advances*, *1*(1), e1400082. https://doi.org/10.1126/sciadv.1400082

Cook, B. I., Cook, E. R., Anchukaitis, K. J., Seager, R., & Miller, R. L. (2011). Forced and unforced variability of twentieth century North American droughts and pluvials. *Climate Dynamics*, *37*(5–6), 1097–1110. https://doi.org/10.1007/s00382-010-0897-9

Cook, B. I., Miller, R. L., & Seager, R. (2009). Amplification of the North American "Dust Bowl" drought through human-induced land degradation. *Proceedings of the National Academy of Sciences*, *106*(13), 4997–5001. https://doi.org/10.1073/pnas.0810200106

Cook, B. I., Seager, R., & Miller, R. L. (2011). Atmospheric circulation anomalies during two persistent North American droughts: 1932–1939 and 1948–1957. *Climate Dynamics*, *36*(11–12), 2339–2355. https://doi.org/10.1007/s00382-010-0807-1

Cook, B. I., Smerdon, J. E., Seager, R., & Cook, E. R. (2014). Pan-continental droughts in North America over the last millennium. *Journal of Climate*, *27*(1), 383–397. https://doi.org/10.1175/JCLI-D-13-00100.1

Cook, E. R., Seager, R., Cane, M. A., & Stahle, D. W. (2007). North American drought: Reconstructions, causes, and consequences. *Earth Science Reviews*, *81*(1–2), 93–134. https://doi.org/10.1016/j.earscirev.2006.12.002

Cook, E. R., Seager, R., Heim, R. R. Jr., Vose, R. S., Herweijer, C., & Woodhouse, C. (2010). Megadroughts in North America: Placing IPCC projections of hydroclimatic change in a long-term palaeoclimate context. *Journal of Quaternary Science*, *25*(1), 48–61. https://doi.org/10.1002/jqs.1303

Cook, E. R., Woodhouse, C. A., Eakin, C. M., Meko, D. M., & Stahle, D. W. (2004). Long-term aridity changes in the western United States. *Science*, *306*(5698), 1015–1018. https://doi.org/10.1126/science.1102586

Dai, S., Shulski, M. D., Hubbard, K. G., & Takle, E. S. (2016). A spatiotemporal analysis of Midwest US temperature and precipitation trends during the growing season from 1980 to 2013. *International Journal of Climatology*, *36*(1), 517–525. https://doi.org/10.1002/joc.4354

De Jonge, C., Hopmans, E. C., Zell, C. I., Kim, J.-H., Schouten, S., & Sinninghe Damsté, J. S. (2014). Occurrence and abundance of 6-methyl branched glycerol dialkyl glycerol tetraethers in soils: Implications for palaeoclimate reconstruction. *Geochimica et Cosmochimica Acta*, *141*, 97–112. https://doi.org/10.1016/j.gca.2014.06.013

Dee, S. G., Parsons, L. A., Loope, G. R., Overpeck, J. T., Ault, T. R., & Emile-Geay, J. (2017). Improved spectral comparisons of paleoclimate models and observations via proxy system modeling: Implications for multi-decadal variability. *Earth and Planetary Science Letters*, *476*, 34–46. https://doi.org/10.1016/j.epsl.2017.07.036

Dirmeyer, P. A., & Kinter, J. L. III (2009). The "Maya Express": Floods in the US Midwest. *Eos, Transactions American Geophysical Union*, *90*(12), 101–102. https://doi.org/10.1029/2009EO120001

Easterling, D. R., Kunkel, K. E., Arnold, J. R., Knutson, T., LeGrande, A. N., Leung, L. R., et al. (2017). Precipitation change in the United States. In K. A. Fahey, D. J. Hibbard, B. C. Dokken, D. J. Stewart, D. W. Wuebbles, & T. K. Maycock (Eds.), *Climate science special report: Fourth national climate assessment* (Vol. 1, pp. 207–230). Washington, DC: U.S. Global Change Research Program. https://doi.org/10.7930/J0H993CC

Eglinton, G., & Hamilton, R. J. (1967). Leaf epicuticular waxes. *Science*, *156*(3780), 1322–1335. https://doi.org/10.1126/science.156.3780.1322

Feng, S., Oglesby, R. J., Rowe, C. M., Loope, D. B., & Hu, Q. (2008). Atlantic and Pacific SST influences on Medieval drought in North America simulated by the Community Atmospheric Model. *Journal of Geophysical Research*, *113*, D11101. https://doi.org/10.1029/2007JD009347

Forman, S. L., Marín, L., Gomez, J., & Pierson, J. (2008). Late Quaternary eolian sand depositional record for southwestern Kansas: Landscape sensitivity to droughts. *Palaeogeography, Palaeoclimatology, Palaeoecology*, *265*(1–2), 107–120. https://doi.org/10.1016/j.palaeo.2008.04.028

Hanson, P. R., Arbogast, A. F., Johnson, W. C., Joeckel, R. M., & Young, A. R. (2010). Megadroughts and late Holocene dune activation at the eastern margin of the Great Plains, north-central Kansas, USA. *Aeolian Research*, *1*(3–4), 101–110. https://doi.org/10.1016/j.aeolia.2009.10.002

Hanson, P. R., Joeckel, R. M., Young, A. R., & Horn, J. (2009). Late Holocene dune activity in the Eastern Platte River Valley, Nebraska. *Geomorphology*, *103*(4), 555–561. https://doi.org/10.1016/j.geomorph.2008.07.018

Harden, T. M., O'Connor, J. E., & Driscoll, D. G. (2015). Late Holocene flood probabilities in the Black Hills, South Dakota with emphasis on the Medieval Climate Anomaly. *Catena*, *130*, 62–68. https://doi.org/10.1016/j.catena.2014.10.002

Hopmans, E. C., Schouten, S., & Damsté, J. S. S. (2016). The effect of improved chromatography on GDGT-based palaeoproxies. *Organic Geochemistry*, *93*, 1–6.

Knox, J. C. (1988). Climatic influence on upper Mississippi valley floods. In V. R. Baker, R. C. Kochel, & P. C. Patton (Eds.), *Flood geomorphology* (pp. 279–300). New York, NY: John Wiley & Sons.

Kunkel, K. E., Changnon, S. A., & Angel, J. R. (1994). Climatic aspects of the 1993 upper Mississippi River basin flood. *Bulletin of the American Meteorological Society*, *75*(5), 811–822. https://doi.org/10.1175/1520-0477(1994)075<0811:CAOTUM>2.0.CO;2

Lee, H., Feakins, S. J., Lu, Z., Schimmelmann, A., Sessions, A. L., Tierney, J. E., & Williams, T. J. (2017). Comparison of three methods for the methylation of aliphatic and aromatic compounds. *Rapid Communications in Mass Spectrometry*, *31*(19), 1633–1640. https://doi.org/10.1002/rcm.7947

Mason, J. A., Swinehart, J. B., Goble, R. J., & Loope, D. B. (2004). Late-Holocene dune activity linked to hydrological drought, Nebraska Sand Hills, USA. *The Holocene*, *14*(2), 209–217. https://doi.org/10.1191/0959683604hl677rp

McQueen, K. C., Vitek, J. D., & Carter, B. J. (1993). Paleoflood analysis of an alluvial channel in the south-central Great Plains: Black Bear Creek, Oklahoma. *Geomorphology*, *8*(2–3), 131–146. https://doi.org/10.1016/0169-555X(93)90033-X

Miao, X., Mason, J. A., Swinehart, J. B., Loope, D. B., Hanson, P. R., Goble, R. J., & Liu, X. (2007). A 10,000 year record of dune activity, dust storms, and severe drought in the central Great Plains. *Geology*, *35*(2), 119–122. https://doi.org/10.1130/G23133A.1

Milly, P. C. D., Wetherald, R. T., Dunne, K. A., & Delworth, T. L. (2002). Increasing risk of great floods in a changing climate. *Nature*, *415*(6871), 514–517. https://doi.org/10.1038/415514a

Munoz, S. E., & Dee, S. G. (2017). El Niño increases the risk of lower Mississippi River flooding. *Scientific Reports*, *7*(1), 1772. https://doi.org/10.1038/s41598-017-01919-6

Munoz, S. E., Giosan, L., Blusztajn, J., Rankin, C., & Stinchcomb, G. E. (2019). Radiogenic fingerprinting reveals anthropogenic and buffering controls on sediment dynamics of the Mississippi River system. *Geology*, *47*(3), 271–274. https://doi.org/10.1130/G45194.1

Munoz, S. E., Giosan, L., Therrell, M. D., Remo, J. W. F., Shen, Z., Sullivan, R. M., et al. (2018). Climatic control of Mississippi River flood hazard amplified by river engineering. *Nature*, *556*(7699), 95–98. https://doi.org/10.1038/nature26145

Munoz, S. E., Gruley, K. E., Massie, A., Fike, D. A., Schroeder, S., & Williams, J. W. (2015). Cahokia's emergence and decline coincided with shifts of flood frequency on the Mississippi River. *Proceedings of the National Academy of Sciences*, *112*(20), 6319–6324. https://doi.org/10.1073/pnas.1501904112

Munoz, S. E., Schroeder, S., Fike, D. A., & Williams, J. W. (2014). A record of sustained prehistoric and historic land use from the Cahokia region, Illinois, USA. *Geology*, *42*(6), 499–502. https://doi.org/10.1130/G35541.1

National Weather Service, NWS. (2020). Climatological data for St. Louis, Columbia, and Quincy. URL: https://www.weather.gov/lsx/cli_archive

Nusbaumer, J., Alexander, P. M., LeGrande, A. N., & Tedesco, M. (2019). Spatial shift of Greenland moisture sources related to enhanced Arctic warming. *Geophysical Research Letters*, *46*, 14,723–14,731. https://doi.org/10.1029/2019GL084633

Parsons, L. A., Loope, G. R., Overpeck, J. T., Ault, T. R., Stouffer, R., & Cole, J. E. (2017). Temperature and precipitation variance in CMIP5 simulations and paleoclimate records of the last millennium. *Journal of Climate*, *30*(22), 8885–8912. https://doi.org/10.1175/JCLI-D-16-0863.1

Peterson, T. C., Heim, R. R. Jr., Hirsch, R., Kaiser, D. P., Brooks, H., Diffenbaugh, N. S., et al. (2013). Monitoring and understanding changes in heat waves, cold waves, floods, and droughts in the United States: State of knowledge. *Bulletin of the American Meteorological Society*, *94*(6), 821–834. https://doi.org/10.1175/BAMS-D-12-00066.1

Pinter, N., Jemberie, A. A., Remo, J. W., Heine, R. A., & Ickes, B. S. (2008). Flood trends and river engineering on the Mississippi River system. *Geophysical Research Letters*, *35*, L23404. https://doi.org/10.1029/2008GL035987

Qiao, L., Pan, Z., Herrmann, R. B., & Hong, Y. (2014). Hydrological variability and uncertainty of lower Missouri river basin under changing climate. *JAWRA Journal of the American Water Resources Association*, *50*(1), 246–260. https://doi.org/10.1111/jawr.12126

Rozanski, K., Araguas-Araguas, L., & Gonfiantini, R. (1993). Isotopic patterns in modern global precipitation. In P. K. Swart, K. C. Lohmann, J. McKenzie, & S. Savin (Eds.), *Climate change in continental isotopic records Geophysical Monograph 78* (pp. 1–36). Washington, DC: American Geophysical Union.

Russell, J. M., Hopmans, E. C., Loomis, S. E., Liang, J., & Sinninghe Damsté, J. S. (2018). Distributions of 5- and 6-methyl branched glycerol dialkyl glycerol tetraethers (brGDGTs) in East African lake sediment: Effects of temperature, pH, and new lacustrine paleotemperature calibrations. *Organic Geochemistry*, *117*, 56–69. https://doi.org/10.1016/j.orggeochem.2017.12.003

Sachse, D., Billault, I., Bowen, G. J., Chikaraishi, Y., Dawson, T. E., Feakins, S. J., et al. (2012). Molecular paleohydrology: Interpreting the hydrogen isotopic composition of lipid biomarkers from photosynthesizing organisms. *Annual Review of Earth and Planetary Sciences*, *40*(1), 221–249. https://doi.org/10.1146/annurev-earth-042711-105535

Schmidt, G. A., Kelley, M., Nazarenko, L., Ruedy, R., Russell, G. L., Aleinov, I., et al. (2014). Configuration and assessment of the GISS ModelE2 contributions to the CMIP5 archive. *Journal of Advances in Modeling Earth Systems*, *6*, 141–184. https://doi.org/10.1002/2013MS000265

Schneider, U., Becker, A., Finger, P., Meyer-Christoffer, A., Rudolf, B., Ziese, M. (2011). GPCC full data reanalysis version 6.0 at 1.0°: Monthly land-surface precipitation from rain-gauges built on GTS-based and historic data, https://doi.org/10.5676/DWD_GPCC/FD_M_V7_100

Seager, R., Kushnir, Y., Herweijer, C., Naik, N., & Velez, J. (2005). Modeling of tropical forcing of persistent droughts and pluvials over western North America: 1856–2000. *Journal of Climate*, *18*(19), 4065–4088. https://doi.org/10.1175/JCLI3522.1

Shadie, C. E., Lopez-Llompart, P., Samet, M., Strole, T., & Kondolf, G. M. (2018). Managing floods in large river basins in the USA: The Mississippi River. In A. Serra-Llobet, G. M. Kondolf, K. Schaefer, & S. Nicholson (Eds.), *Managing Flood Risk* (pp. 11–41). Cham: Palgrave Macmillan. https://doi.org/10.1007/978-3-319-71673-2

Sjostrom, D. J., & Welker, J. M. (2009). The influence of air mass source on the seasonal isotopic composition of precipitation, eastern USA. *Journal of Geochemical Exploration*, *102*(3), 103–112. https://doi.org/10.1016/j.gexplo.2009.03.001

Steiger, N. J., Smerdon, J. E., Cook, B. I., Seager, R., Williams, A. P., & Cook, E. R. (2019). Oceanic and radiative forcing of medieval megadroughts in the American Southwest. *Science Advances*, *5*(7), eaax0087. https://doi.org/10.1126/sciadv.aax0087

Stevenson, S., Otto-Bliesner, B. L., Brady, E. C., Nusbaumer, J., Tabor, C., Tomas, R., et al. (2019). Volcanic eruption signatures in the isotope-enabled last millennium ensemble. *Paleoceanography and Paleoclimatology*, *34*(8), 1534–1552. https://doi.org/10.1029/2019PA003625

Tao, B., Tian, H., Ren, W., Yang, J., Yang, Q., He, R., et al. (2014). Increasing Mississippi River discharge throughout the 21st century influenced by changes in climate, land use, and atmospheric CO_2. *Geophysical Research Letters*, *41*, 4978–4986. https://doi.org/10.1002/2014GL060361

Tian, C., Wand, L., Kaseke, K. F., & Bird, B. W. (2018). Stable isotope compositions (δ^2H, $\delta^{18}O$ and $\delta^{17}O$) of rainfall and snowfall in the central United States. *Scientific Reports*, *8*(1), 6712. https://doi.org/10.1038/s41598-018-25102-7

Wang, L., & Leigh, D. S. (2012). Late-Holocene paleofloods in the Upper Little Tennessee River valley, Southern Blue Ridge Mountains, USA. *The Holocene*, *22*(9), 1061–1066. https://doi.org/10.1177/0959683612437863

White, A. J., Stevens, L. R., Lorenzi, V., Munoz, S. E., Lipo, C. P., & Schroeder, S. (2018). An evaluation of fecal stanols as indicators of population change at Cahokia, Illinois. *Journal of Archaeological Science*, *93*, 129–134. https://doi.org/10.1016/j.jas.2018.03.009

White, A. J., Stevens, L. R., Lorenzi, V., Munoz, S. E., Schroeder, S., Cao, A., & Bogdanovich, T. (2019). Fecal stanols show simultaneous flooding and seasonal precipitation change correlate with Cahokia's population decline. *Proceedings of the National Academy of Sciences*, *116*(12), 5461–5466. https://doi.org/10.1073/pnas.1809400116

Williams, J. W., & Jackson, S. T. (2003). Palynological and AVHRR observations of modern vegetational gradients in eastern North America. *The Holocene*, *13*(4), 485–497. https://doi.org/10.1191/0959683603hl613rp

Wise, E. K., Woodhouse, C. A., McCabe, G. J., Pederson, G. T., & St-Jacques, J. M. (2018). Hydroclimatology of the Missouri River Basin. *Journal of Hydrometeorology*, *19*(1), 161–182. https://doi.org/10.1175/JHM-D-17-0155.1

Woodhouse, C. A., & Overpeck, J. T. (1998). 2000 years of drought variability in the central United States. *Bulletin of the American Meteorological Society*, *79*(12), 2693–2714. https://doi.org/10.1175/1520-0477(1998)079<2693:YODVIT>2.0.CO;2